Behavioral/Systems/Cognitive

Independent Projection Streams from Macaque Striate Cortex to the Second Visual Area and Middle Temporal Area

Lawrence C. Sincich and Jonathan C. Horton
Beckman Vision Center, University of California, San Francisco, San Francisco, California 94143

The interareal wiring of the neocortex is usually depicted as a network of single point-to-point connections, often side-stepping the possibility that some neurons may project to multiple cortical areas. The prevalence of such neurons is unknown; if they are abundant, cortical circuits are more likely to be connectionally diffuse. We used a dual-tracer approach to determine whether single neurons in the macaque primary visual cortex (V1) project to two extrastriate areas, the second visual area (V2) and the middle temporal area (MT). We found two large intermingled groups of single-labeled neurons in layer 4B of V1 projecting independently to either V2 or MT. A third, sparser group of double-labeled neurons projected to both areas; we termed these manifold neurons. We also found that MT-projecting cells were distributed indiscriminately with respect to cytochrome oxidase compartment in layer 4B, revealing a subpopulation that provides a potential source of patch input from V1 to MT. The results demonstrate that primary sensory cortices can use multiple projection strategies to distribute signals to higher areas, and suggest that feedforward projections may route signals with more specificity than feedback pathways.

Key words: **visual cortex; intracortical; manifold projections; flatmount; motion; cytochrome oxidase; patch column; interpatch column**

Introduction

The occipital, temporal, and parietal lobes of the cerebral cortex harbor a large number of cortical areas that respond to visual stimuli. On average, each area is connected to 15 others in the macaque brain (Felleman and Van Essen, 1991). This invites the question: do typical cortical neurons project to 15 areas, a few areas, or just one? Decades of mapping connections with single tracers have provided a basic interareal wiring diagram of the cortex. However, the use of single tracers cannot easily reveal whether a given neuron projects to multiple areas (Giolli and Towns, 1980; Bullier and Kennedy, 1987; Barbas, 1995). Single feedback axons have been reconstructed, showing that some neurons do project to multiple areas (Rockland and Drash, 1996; Rockland and Knutson, 2000), but the strategies used by feedback and feedforward projections may not be the same (Weller and Kaas, 1983; Krubitzer and Kaas, 1989; Salin and Bullier, 1995). Few studies have used multiple tracers to address this issue for feedforward intrahemispheric projections in primates (Schwartz and Goldman-Rakic, 1984; Nakamura et al., 1993). One study in the cat has shown that 1–3% of area 17 neurons projects to both areas 18 and 19 (Bullier et al., 1984). It is likely that single projection neurons also target multiple areas in macaque visual cortex, but their prevalence is not known.

Surprisingly, neuroanatomists have not agreed on a term to distinguish cortical neurons that project to a single area versus multiple areas (Lockard, 1992). We propose the term "manifold" for neurons that send an axon branch to at least two different cortical areas and the term "solitary" for neurons that project to just one area. If manifold neurons are rare, then most information in the cortex must be transmitted by solitary neurons. If so, are there multiple classes of solitary neurons that handle the projections to multiple areas? This question, like the issue of manifold neurons, cannot be addressed with a single retrograde tracer.

The existence of feedforward manifold neurons, or multiple classes of solitary neurons, requires injection of different retrograde tracers into corresponding loci within different target cortical areas. For example, in the visual system, injections must be made into recipient cortical areas at identical points in each retinotopic map. Furthermore, the cortical areas in question must be well accepted, accessible, and identifiable. The primary visual cortex (striate cortex, or V1) is ideally suited for revealing patterns of feedforward projections. It contains cells in layer 4B that project to the second visual area (V2) and middle temporal area (MT, or V5) (Lund et al., 1975; Maunsell and Van Essen, 1983; Ungerleider and Desimone, 1986; Shipp and Zeki, 1989; Sincich and Horton, 2002a). The retinotopic organization in V1, V2, and MT has been mapped previously, and the areas have characteristic patterns of cytochrome oxidase (CO) staining that make them recognizable in tissue sections. The cortical targets of projection neurons in layer 4B, whether solitary or manifold, cannot be determined by cell morphology alone (Shipp and Zeki, 1989).

We used a dual-tracer technique to map the projections of layer 4B neurons in V1 to areas V2 and MT in the macaque (Sincich and Horton, 2002c). Most retrogradely filled cells were single labeled, closely interspersed within layer 4B and residing in both patch and interpatch CO compartments. The projections from V1 to V2 and MT are therefore substantially exclusive, despite arising from the same V1 layer. A subpopulation of the MT-projecting neurons in layer 4B provides the only possible

Received Jan. 2, 2003; revised April 9, 2003; accepted April 11, 2003.

This work was supported by National Eye Institute Grants EY10217 (J.C.H.), EY13676 (L.C.S.), and EY02162 (Beckman Vision Center). Support was also received from That Man May See, The Bunter Fund, and Research to Prevent Blindness (J.C.H.). The California Regional Primate Research Center is supported by National Institutes of Health Base Grant RR00169. We thank D. L. Adams, J. A. Movshon, and H. L. Read for their comments on this manuscript.

Correspondence should be addressed to Dr. Lawrence C. Sincich, Beckman Vision Center, University of California, San Francisco, 10 Koret Way, San Francisco, CA 94143-0730. E-mail: sincich@itsa.ucsf.edu.

 0270-6474/03/235684-09$15.00/0

direct source of CO patch output from V1, which may convey color signals. Double-labeled manifold neurons were present but sparse, forming a minority of V1 cells that provide identical information to V2 and MT. Thus, V1 may convey at least three different visual signals from layer 4B, with segregated solitary projections being the most prevalent feedforward strategy at this juncture in the visual pathway. If other cortical areas use similar projection strategies, then wiring schemes of the neocortex must be reconfigured to account for the presence of manifold pathways.

Materials and Methods

Experimental animals and surgical procedures. Experiments were conducted in four adult male *Macaca fascicularis* using procedures approved by the University of California, San Francisco Committee on Animal Research and in accordance with National Institutes of Health guidelines. Anesthesia was induced with ketamine HCl (10 mg/kg, i.m.). The animal was intubated endotrachially and anesthesia was maintained with 1.5% isoflurane in a 1:1 mixture of N_2O:O_2. We monitored electrocardiogram, respiratory rate, body temperature, blood oxygenation (S_pO_2), endtidal CO_2, and inspired/expired levels of anesthetic gases throughout the experiment. A 5% dextrose in half-normal saline solution was given intravenously at 3 ml/kg per hour. After the animal was placed in a stereotaxic frame, a craniotomy was made to expose the lunate and superior temporal sulci. The dura was widely reflected to make sulci obvious.

Retrograde tracers were reconstituted in filtered, sterile balanced salt solution. For MT injections along each of six to seven penetrations, four 120 nl pressure injections of 0.1% gold-conjugated cholera toxin B subunit (CTB; List Biologic, Campbell, CA) (Llewellyn-Smith et al., 1990) were made every 1.5 mm at depths between 7 and 11.5 mm into the posterior bank of the superior temporal sulcus (STS) (Ungerleider and Mishkin, 1979; Gattass and Gross, 1981; Van Essen et al., 1981; Weller and Kaas, 1983). The angle of approach was roughly sagittal but was adjusted to account for variation in gross cortical anatomy according to our experience. Beginning 18 mm from the midline, we spaced the pipette penetrations 2 mm apart in a zig-zag line moving laterally (for entry points on the prelunate gyrus, see Fig. 2*d*,*e*). For V2 injections, 9–12 60 nl pressure injections of 4% wheat-germ agglutinin (WGA) conjugated to horseradish peroxidase (HRP) (L-3892; Sigma, St. Louis, MO) were placed 3 mm apart along the posterior lip of the lunate sulcus, each at a depth of 600 μm. After completing the injections, the dura was sutured and the bone flap was replaced. We repeated the injections in the other hemisphere. Buprenorphine (0.02 mg/kg i.m.) was administered postoperatively every 8 hr until the animal recovered from surgery.

The injections were placed successfully in four hemispheres of three animals. In the remaining two hemispheres, and in both hemispheres of the fourth monkey, the injections did not produce overlapping label either because CTB was deposited in dorsal MT, leading to retrograde labeling in the wrong portion of V1, or because the WGA–HRP injections intended for V2 strayed into V1.

The monkey shown in Figure 1 is from a series of experiments examining the correlation between CO stripes in V2 and the projections from V1 in macaques (Sincich and Horton, 2002b). We used tritiated proline injections to anterogradely label the axons of V1 neurons projecting to extrastriate cortex. In all 10 hemispheres of this study, we found terminal fields labeled in V2 and MT, with no evidence of secondary areas near MT in the STS that received direct input from V1. However, weak projections may not have been revealed with the autoradiographic exposures we used. The labeled fields were used as additional guides for the placement of CTB injections in MT and to provide assurance that no region immediately surrounding MT might transport stray tracer to V1.

Histology. After 2–3 d for transport, the animals were given a lethal dose of pentobarbital (150 mg/kg) and cardially perfused with 2 L of 0.9% saline followed by 1 L of 1% paraformaldehyde in 0.1 M phosphate buffer (PB), pH 7.4. The brain was removed and flatmounts were prepared containing V1 and the cortex within the lunate sulcus and STS (Olavarria and Van Sluyters, 1985). The flatmounts were left overnight in 1.33% paraformaldehyde plus 30% sucrose in PB at room temperature under light pressure ($\sim$4 gm/cm^2). We cut frozen sections parallel to the pial surface, alternating between 25 μm thick for CO processing (Wong-Riley, 1979) and 75 μm for CTB/WGA–HRP histochemistry (Sincich and Horton, 2002a). Silver intensification of CTB was done with the IntenSE-M kit (Amersham Biosciences, Little Chalfont, UK). CO-stained sections were photographed before processing for CTB. Sulcal boundaries were traced from the first sections, which retain the arachnoid membranes that were cut to initially open the sulci in the intact brain. We also photographed the brains during unfolding to keep track of the gross anatomical landmarks.

Data analysis. In all four analyzed cases, there was heavy CTB labeling in opercular V1, including areas near the border with V2. For cell counting, labeled cells were plotted by camera lucida at 400× magnification. In flattened CTB/WGA–HRP-stained material, layer 4B cells were usually captured in a single section. Multiple (5–12) 0.25 mm^2 fields in each hemisphere were selected for cell counting in layer 4B. These fields were opposite V2 injections in all three stripe types, often straddling the stripes. We surveyed each section at low magnification to locate the portion of each section where the density of cells labeled by each tracer overlapped maximally. Selecting such regions for high magnification analysis optimized the likelihood of detecting double-labeled cells. We used the CO pattern to identify cortical layers; in all cases, layer 4A was superficial to the CTB-labeled cells. The density of labeled cells varied between animals, primarily because double-labeled regions did not necessarily contain the densest population of any one label, and because histological processing is inherently variable. Single-labeled cells in one-third of every counted field and all double-labeled cells were outlined for cell body area measurements. These outlines were transferred into Illustrator 9.0 (Adobe Systems, San Jose, CA) to calculate areas using the CADtools 2.1 extension (Hot Door, Grass Valley, CA).

Cell morphology is not readily determined in tangential sections. In many cases, we could not decide whether a cell was one of two known morphologies, stellate or pyramidal. However, in particularly well labeled cells, apical dendrites could be observed by focusing through the section. Pyramidal cells often had three basal dendrites, giving them a triangular appearance in the top-down view (see Fig. 5*b*,*d*). In contrast, stellates had more compact cells bodies, with less tapering at the start of their lateral dendrites. Because weak labeling would lead to the underestimation of pyramidal cells, we did not quantify the proportion of pyramidal versus stellate cells.

To quantify the relationship between MT-projecting neurons and CO patches, we analyzed only areas in which CTB-labeled cell density was high. We aligned digital images of sections from layer 3 and 4B with Photoshop 6.0 (Adobe Systems) using blood vessels as guides. Minor scaling and no warping were needed for alignment. Vessel profiles in the layer 3 CO image were filled in with the mean image luminance. A low-pass Fourier-filtered version of this image (cutoff frequency, 1.1 cycles/mm) was subtracted from the original to produce a gray-level flattened version of the CO pattern. This image was blurred with a Gaussian filter ($\sigma = 70$ μm). To produce a spatial average of the CO values surrounding MT-projecting cells similar to that of Boyd and Casagrande (1999), a 340 × 340 μm region centered on the position of each labeled cell was summed for all cells in the field (except those within 170 μm of the border). The gray range of the spatial average was multiplied by 40 to heighten contrast. This analysis was performed on one $\sim$12 mm^2 field in each monkey. Each field was taken from a different eccentricity to control for possible foveal versus peripheral variation. In a separate analysis, the processed CO image was divided into three gray levels (patch, border, interpatch), each occupying one-third of the image area. A three-way χ^2 test was used to determine whether the distribution of cells among these three gray levels differed significantly from chance. Analysis routines were written in MatLab 5.0 (MathWorks, Natick, MA).

Results

To guide the placement of tracers into retinotopically corresponding locations in V2 and MT, we first mapped the terminal fields of V1 neurons projecting to these extrastriate areas. We subsequently verified the location of the cortical areas postmor-

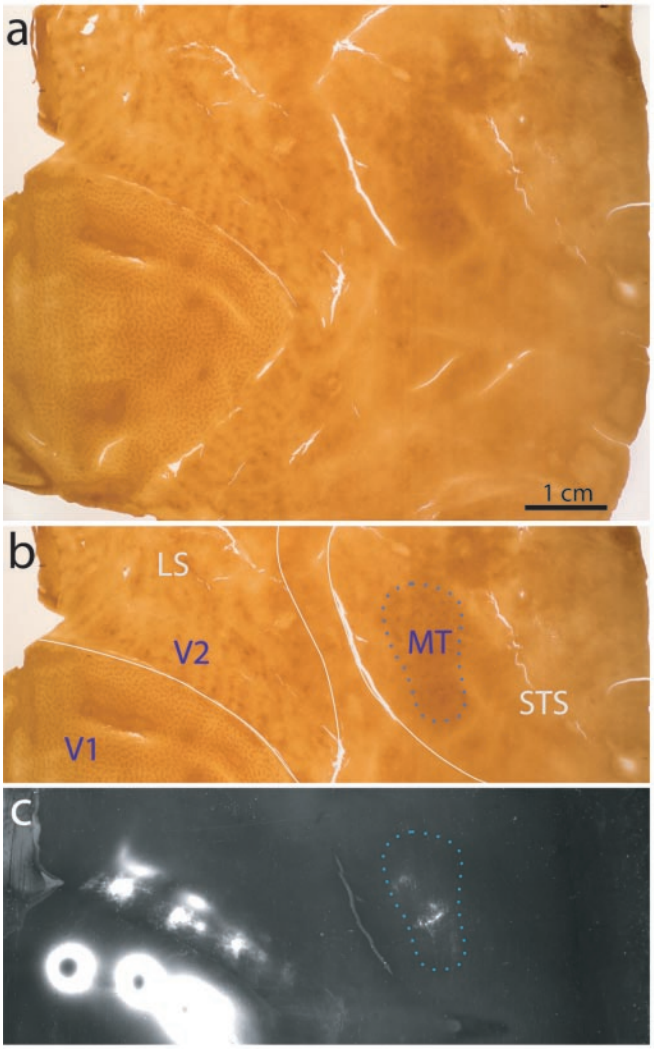

Figure 1. Location of V1 projection zones in V2 and MT. *a*, Single flatmount section cut through the superficial layers of the right occipital cortex of a macaque, showing the CO pattern in V1, V2, and MT. *b*, Same section as in *a* with areas identified and sulci outlined in white. Sulcal boundaries are tracked during the unfolding process. The blue dotted line indicates area MT as judged by the CO pattern. *c*, Adjacent section to *a*, processed for autoradiography and photographed in dark-field. The large [^{3}H]proline injections in V1 lead to anterogradely labeled fields of axon terminals centered in V2 and MT. Scale bar, 1 cm.

tem by staining the tissue for CO. V1, V2, and MT are all recognizable in CO sections if the cortex is unfolded and flattened before histological processing (Fig. 1*a*). V1 contains the characteristic rows of CO patches (Horton and Hubel, 1981), V2 is identified by the series of pale-thin-pale-thick CO stripes running perpendicular to the V1–V2 border (Tootell et al., 1983), and MT can be recognized as a mottled CO pattern within the superior temporal sulcus (Tootell and Taylor, 1995). The anterogradely labeled terminal fields produced by [^{3}H]proline injections in V1 coincided with the locations of the V2 and MT CO patterns (Fig. 1*b*,*c*). In all cases (n = 10 hemispheres), V2 was found in the posterior bank of the lunate sulcus (LS), and MT was located within the posterior bank of the STS, in agreement with previous studies (Cragg, 1969; Zeki, 1969; Ungerleider and Mishkin, 1979; Van Essen et al., 1981). No other terminal labeling was found in the STS, suggesting that the primary area in this sulcus that received input from V1 is MT. Figure 1*c* also demonstrates that V2 is more densely innervated than MT.

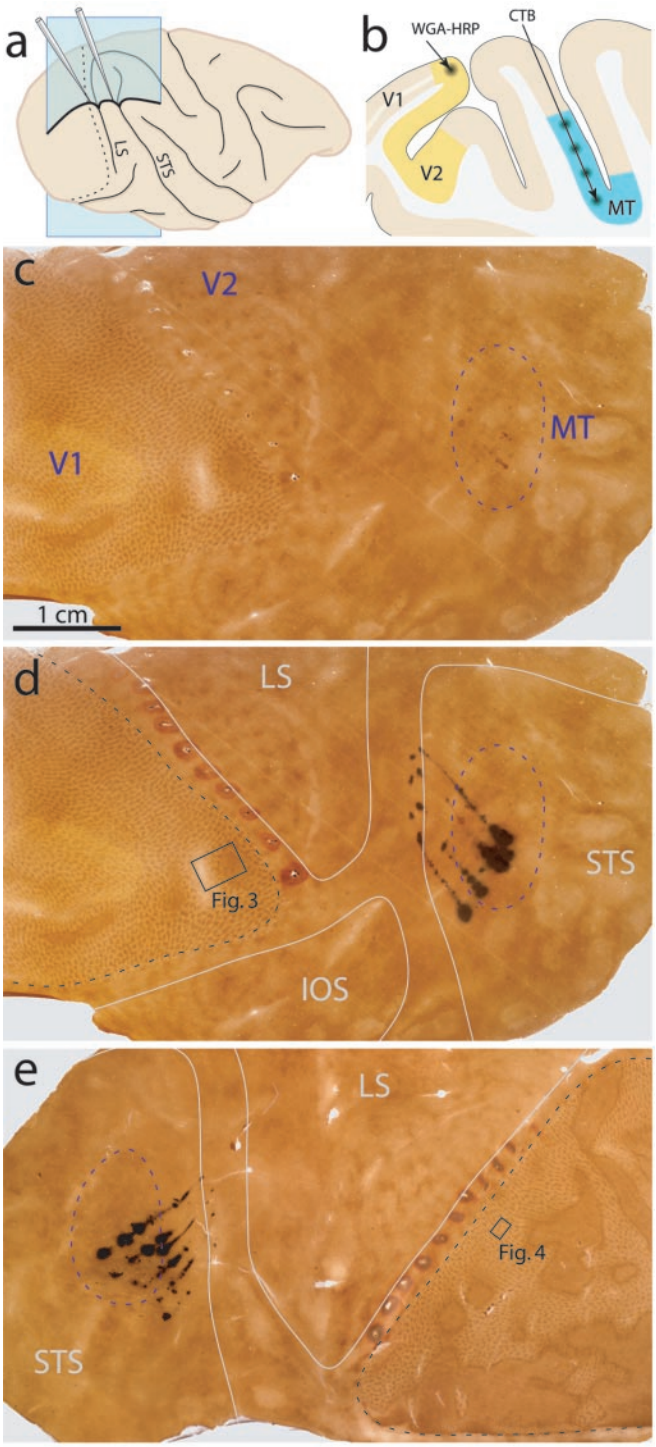

Figure 2. Injection locations in V2 and MT. *a*, Lateral view of a macaque right hemisphere, illustrating pipette entry points. The blue sagittal plane is diagrammed in *b*. The dotted line is the V1–V2 border. *b*, Tracer deposit sites for WGA–HRP in V2 and CTB in MT, as they might appear in a sagittal section. *c*, Single flatmount section from the right hemisphere of Monkey 2. The blue dashed line encircles MT, as estimated from the entire series of sections. Anatomical axes: posterior–anterior, left–right; dorsal–ventral, top– bottom. *d*, Same section as in *c*, with the injection sites from an adjacent CTB/WGA–HRP-reacted section aligned and superimposed digitally. Sulci outlines are drawn in white (IOS, inferior occipital sulcus). The black box outlines the region in which a deeper section was photographed for Figure 3. *e*, Left hemisphere of Monkey 1, with sulcal outlines and injection sites. The black box is a region in V1 in which overlapping labeled cells appeared in a deeper layer 4B section (shown at higher magnification in Figure 4). Scale bar, 1 cm.

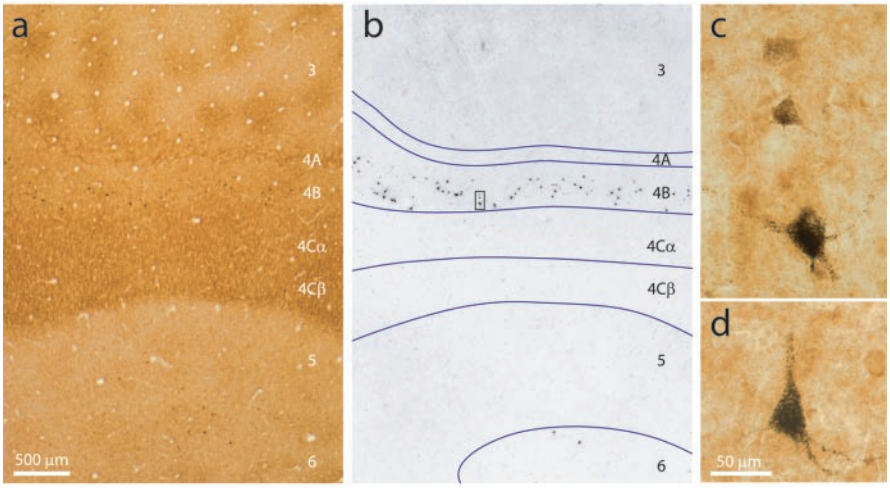

Figure 3. MT-projecting cells in V1. *a*, Brightfield image of a CO-stained section containing CTB-labeled cells. Many layers are visible in this area because the plane of section was oblique to the cortical surface. *b*, Inverted dark-field image of the same section in *a*, showing that CTB labeling was found only in layers 4B and 6. Laminar boundaries (blue) are taken from the CO pattern. *c*, High magnification view of the boxed field in *b*, showing light, medium, and heavily labeled neurons. The two top labeled cells were also CO-rich, as evident in the proximal dendrite staining. *d*, Pyramidal cell from the next section. Its apical dendrite was cut off where it left the section. Stellate cells (*c*, top) had no apical process. Scale bars: *a*, *b*, 500 μm; *c*, *d*, 50 μm.

We used these maps along with sulcal landmarks to guide the retrograde tracer injections into retinotopically similar areas in V2 and MT (Fig. 2*a*). WGA–HRP was injected along a narrow strip of exposed V2, representing parafoveal visual space near the lower vertical meridian (Gattass et al., 1981). As the meridian itself is represented at the V1–V2 border, retrogradely transported WGA–HRP appeared in V1 at a location mirrored across this border. In contrast to V2, MT is completely buried in a sulcus (Fig. 2*b*). We made a series of CTB injections in the posterior bank of the STS, in the MT region that represents the same part of visual space as the V2 injections (Ungerleider and Mishkin, 1979; Gattass and Gross, 1981; Van Essen et al., 1981; Weller and Kaas, 1983).

In four hemispheres from three animals, the two tracers were injected successfully in similar retinotopic locations in V2 and MT (Fig. 2*c–e*). In these cases, the WGA–HRP injections were confined to V2. The CTB injections landed in the ventral MT, in which the central visual field is represented. MT has a vague boundary in CO-stained tissue, making it difficult to be sure the CTB injections were strictly limited to this cortical area. In fact, in several cases, we suspect some CTB landed just outside MT (Fig. 2*d*,*e*). However, two lines of evidence indicate that these extraneous tracer deposits did not contaminate our results. First, CTB-labeled cells in V1 were found exclusively in the lower two-thirds of layer 4B and in upper layer 6 (Fig. 3). These are the same two layers found to project to MT in all previous studies (Lund et al., 1975; Maunsell and Van Essen, 1983; Ungerleider and Desimone, 1986; Shipp and Zeki, 1989). Second, of the cortical areas bordering MT [transitional V4, medial superior temporal (MST), floor of superior temporal, and 7a], only V4 is known to receive a direct projection from V1 (Felleman and Van Essen, 1991). This projection arises from V1 neurons in layer 2–3 (Yukie and Iwai, 1985; Nakamura et al., 1993). Because no labeled neurons were found in layer 2–3 (Fig. 3*b*), no spillage occurred into V4. Peripheral MST may receive a projection from peripheral V1 (Boussaoud et al., 1990). However, this population would not have been counted in our analysis, which was restricted to the area of V1 representing the central 8° of visual space.

Injection of these two tracers gave rise to overlapping fields of labeled neurons in V1, near the dorsal V1–V2 border. High densities of cells filled with WGA–HRP or CTB were intermingled in layer 4B, which is ~110 μm thick. A smaller population of cells was scattered through layer 6. Our analysis concentrates on the more numerous cells in layer 4B.

A survey of a representative field (Fig. 4*a*) from Monkey 1 revealed 897 cells containing WGA–HRP and 78 cells containing CTB. Only six neurons were double labeled (Fig. 4*b*). The density of WGA–HRP cells (598 cells per square millimeter) was extremely high, suggesting that we labeled a high proportion of the cells in the field that projected to V2. The density of the MT-projecting cells (52 per square millimeter) was lower but similar to that reported in a previous study (Shipp and Zeki, 1989). Therefore, the paucity of double-labeled cells was probably not attributable to inadequate labeling of the populations that project to V2 and MT. This point is important, because if only a small percentage of the cells projecting to V2 and MT is labeled successfully, the likelihood of identifying double-labeled cells is reduced.

Double-labeled cells were also scarce in the other three hemispheres (Table 1). The abundance of single-labeled cells in layer 4B showed that neurons representing identical points in visual space project to different visual areas. This raises the possibility that V2 and MT receive input from different cell types. Both pyramidal and stellate cells are known to project from layer 4B to V2 and MT (Tigges et al., 1981; Shipp and Zeki, 1989; Rockland, 1992). The distribution of soma areas of neurons labeled by our injections supported the idea that different cell populations contribute to the three projection streams (Fig. 5). V2-projecting neurons were small pyramidal or stellate cells (median area, 7.5 μm^2) (Fig. 5*a*) and less commonly medium-sized pyramidal cells (Fig. 5*b*). In contrast, MT-projecting neurons were much larger (median area, 19.4 μm^2) and included the distinctive stellate neurons, as described by Meynert (1872) (Fig. 5*c*), as well as many pyramidal cells (Figs. 3*d*, 5*d*). Double-labeled cells were an intermediate size (median area, 15.4 μm^2) and often pyramidal in morphology (Fig. 5*e*,*f*). Determining the true number of pyramidal cells was precluded by partial-cell filling and tangential sectioning. However, apical dendrites, when present, could be recognized by focusing through the tissue. These data provide evidence that the input to V2 and MT comes primarily from segregated V1 populations, but the segregation is not based on a pyramidal versus stellate cell distinction. Frequently, cells labeled with different tracers were located in the same vertical cell column (Fig. 5*g*,*h*). The double-labeled population of medium-sized cells constituted a sparse third population that must convey the same visual signal to both V2 and MT. A nonparametric rank-sum test (Wilcoxon) showed that the double-labeled size distribution was statistically distinct from the two single-labeled populations (double vs CTB, $p = 0.0036$; double vs WGA–HRP, $p < 1 \times 10^{-5}$).

We have shown previously that V1 cells in layer 4B projecting to the thick CO stripes of V2 are clustered into interpatch compartments (Sincich and Horton, 2002a). The thick V2 stripes project, in turn, to area MT (DeYoe and Van Essen, 1985; Shipp and Zeki, 1985). Therefore, one might predict that cells projecting directly from V1 to MT are also concentrated in interpatches. To examine this issue, we compared the distribution of labeled cells with the pattern of CO staining in V1. Although patches are present in layer 4B, they are faint. Therefore, we aligned 4B sections

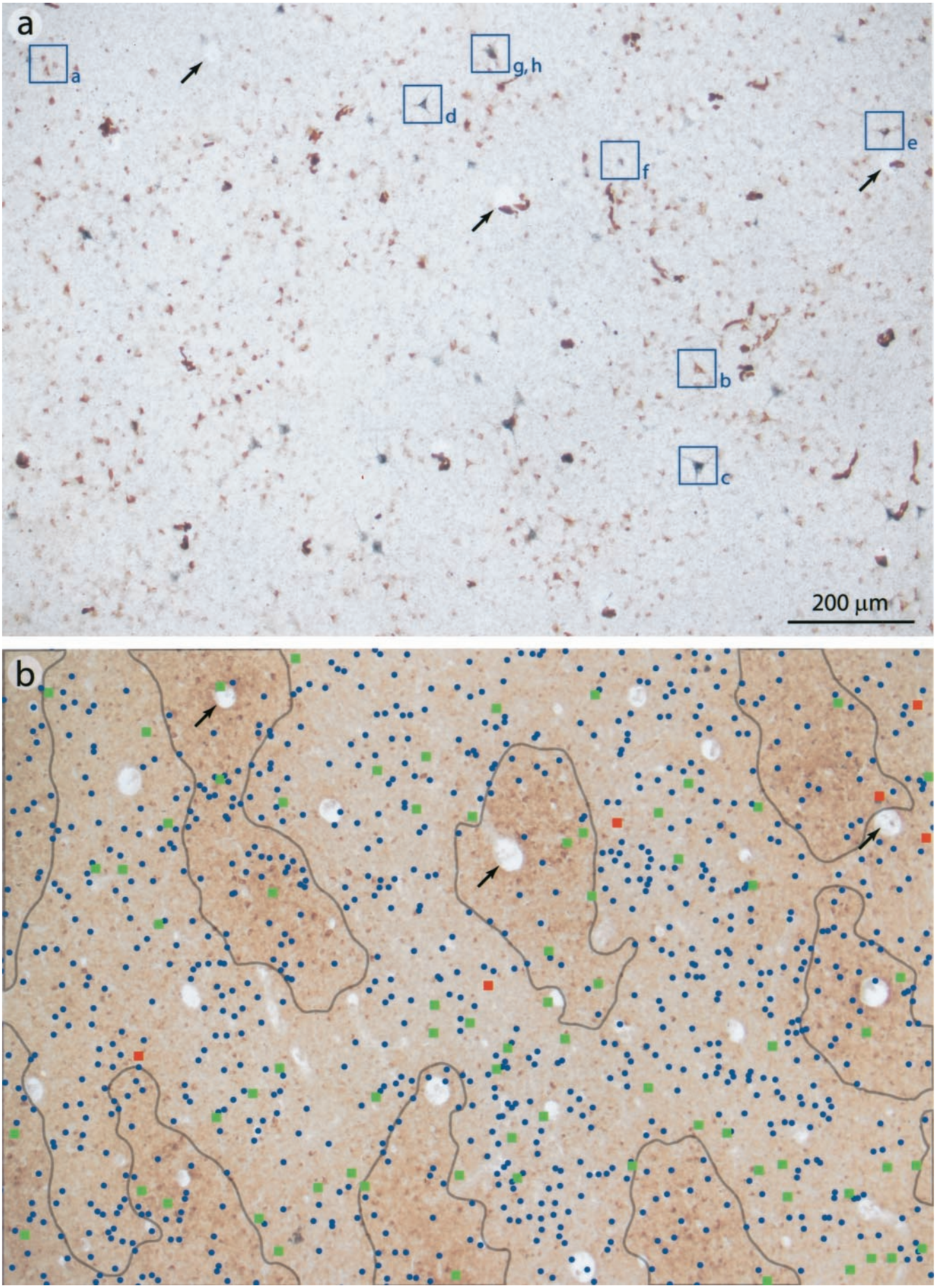
a
a
g, h
d
e
f
b
c
200 μm
b

Table 1. Cells labeled by tracer injections in V2 and MT

Hemisphere	CTB (MT)	WGA–HRP (V2)	Double (percentage of CTB-labled, percentage of WGA-HRP-labeled)	Location of doubles (interpatch, patch)	Area examined (mm^2)
Monkey 1, L	168	1934	17 (9.1, 0.8)	16,1	3
Monkey 2, L	116	203	8 (6.4, 3.8)	7,1	1.5
Monkey 2, R	258	204	11 (4.1, 5.1)	10,1	1.25
Monkey 3, R	47	404	2 (4.1, 0.5)	2,0	1.75
Totals	589	2745	38	35,3*	7.5

*A two-way χ^2 test allotting CO patches one-third of the total V1 area showed that the distribution of double-labeled cells in interpatches was significant ($p < 0.001$).

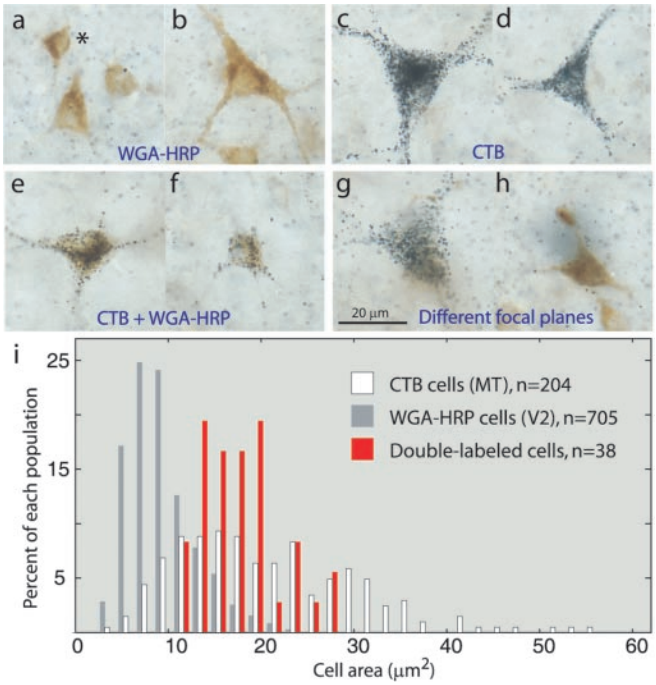

Figure 5. Distinct cell types project to V2 and MT. *a*, *b*, WGA–HRP-labeled cells were most often small stellate (*a*, asterisk) or pyramidal neurons and less frequently medium-sized pyramids (*b*). CTB-labeled neurons included the large Meynert cells characteristic of layer 4B (*c*) and pyramids ranging in size (*d*). *e*, *f*, Double-labeled cells were always medium-sized cells. *g*, *h*, Single-labeled neurons could often be found situated within the same cortical column. *i*, Distribution of cell body areas for each type of labeling across all animals, showing that double-labeled cells (red) formed a subpopulation among the smaller V2-projecting cells (gray) and MT-projecting cells (white). Only one of every three fields were measured for the single-labeled cells. Scale bar: *a*–*h*, 20 μm.

reacted for both WGA–HRP and CTB with CO sections cut through layer 3, in which patches stand out in the highest contrast. Typical fields (Fig. 4*a*,*b*) contained WGA–HRP-labeled cells scattered indiscriminately in both patches and interpatches as expected, because the V2 injections landed in thick, thin, and pale CO stripes (Fig. 2*e*). The CTB-labeled cells also appeared to be distributed randomly with respect to the patch–interpatch system.

Quantitative analysis of the distribution of CTB-labeled cells in each animal confirmed the lack of any tendency for MT-projecting cells to favor patches or interpatches. Figure 6*a* shows a 3 × 4.25 mm field of V1, neighboring the field shown in Figure 4*a* and photographed in dark-field illumination to reveal CTB labeling in layer 4B. The layer 3 CO section aligned with this field (Fig. 6*b*) was gray-level coded and superimposed on a plot of the cells (Fig. 6*c*). Generating a spatial average of the CO density in the tissue surrounding each cell showed that MT-projecting cells did not preferentially reside in patches or interpatches (Fig. 6*d*). This analysis was repeated in three additional hemispheres representing eccentricities from 1 to 15° for a total of 1688 cells. No correlation with CO patches was found at any eccentricity (Fig. 6*d*–*g*) (Shipp and Zeki, 1989), as evident by the noncentered, low-amplitude dark peaks in the spatial correlograms. Randomly shuffling the cell locations within the field produced similar low-amplitude correlograms. A χ^2 analysis comparing the total number of CTB-labeled cells in patches, interpatches, or border regions (Boyd and Casagrande, 1999) also revealed no correlation (Table 2).

Our data indicate that the direct V1 → MT pathway is rooted diffusely in both patches and interpatches, whereas the indirect V1 → V2 thick stripe → MT pathway arises primarily from interpatches (DeYoe and Van Essen, 1985; Shipp and Zeki, 1985; Sincich and Horton, 2002a). This distinction may have functional importance because the direct MT pathway contains a different blend of information, because it incorporates the patches. The manifold population constitutes a third, albeit small pathway. Virtually all of the double-labeled cells that we encountered (35 of 38) were located in interpatches (Table 1). This implies that most manifold cells send one axon branch to V2 thick stripes and the other branch to MT. Such cells convey information both directly and indirectly to area MT. What remains unknown is how signals from these cells carried along one axon branch are modified by intermediate processing in V2.

Discussion

Using a dual-tracer method, we found that V2 and MT receive substantially independent input from V1. Manifold cells were uncommon, despite our efforts to maximize their labeling by choosing populations that cohabit a single layer and injecting retinotopically overlapping locations in V2 and MT. Cell-size differences supported the idea that separate populations project to each extrastriate area.

Our data show that layer 4B neurons play a more diverse role in visual processing than previously thought. In overviews of the visual system, layer 4B has been treated as a single entity, transmitting a magnocellular-dominated motion signal to the extrastriate cortex (Livingstone and Hubel, 1988; Zeki and Shipp, 1988; Van Essen and Gallant, 1994). Mounting evidence instead suggests that layer 4B mediates the distribution of multiple channels of visual information to the extrastriate cortex. Most layer 4B neurons are highly tuned for orientation (Hubel and Wiesel, 1968; Blasdel and Fitzpatrick, 1984). A subset of these oriented cells is selective for direction of motion (Dow, 1974; Schiller et al., 1976; Hawken et al., 1988). These two classes may differ morphologically, perhaps corresponding to the neurons that project to V2 and MT respectively. Stellates, for instance, are the most prevalent type among the MT-projecting cells (Lund et al., 1975;

Figure 4. Three different output populations in layer 4B. *a*, A single section cut tangentially through layer 4B of Monkey 1, processed for WGA–HRP and CTB. Individually lettered neurons are shown at higher magnification in Figure 5. *b*, Desaturated image of the CO pattern in layer 3, showing the distribution of labeled cells in a in patch (gray outline) and interpatch compartments. Blue dots indicate WGA–HRP-labeled cells projecting to V2, green squares indicate CTB cells projecting to MT, and red squares indicate double-labeled cells. Black arrows point to blood vessels used for alignment. Scale bar, 200 μm.

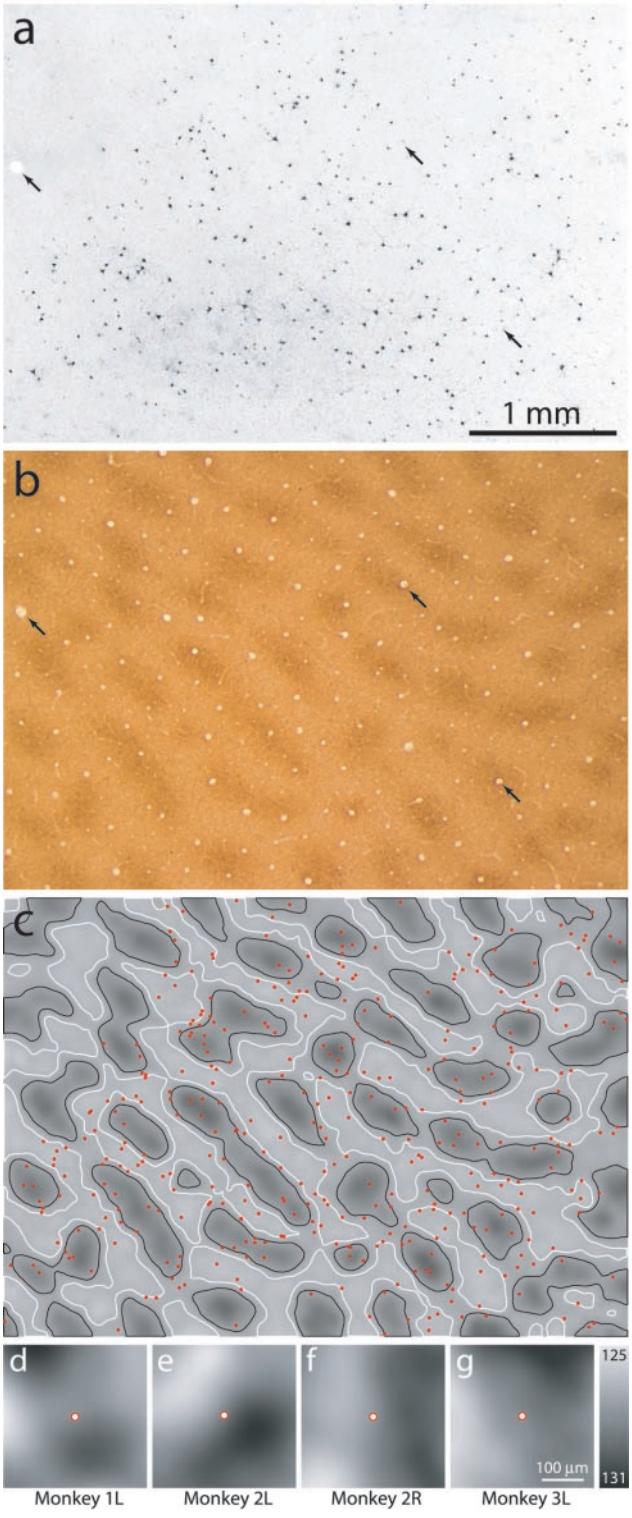

Figure 6. MT-projecting cells are independent of the CO patch system. *a*, Inverted dark-field image of CTB-labeled cells in layer 4B. The top left corner of the section passed out of layer 4B. Black arrows point to blood vessels used for alignment. *b*, CO section from layer 3 aligned with the section in *a*. *c*, Gray-level rendered image of CO density, divided into three zones of equal area for χ^2 analysis: patch (inside black contours), border (between black and white contours), and interpatch. Cells (red) plotted over the density image from *a*, showing no tendency to cluster in any zone. Spatial correlation analysis showed that the mean CO density in the neighborhood of MT-projecting cells was not clearly related to patches in this case (*d*), nor in three other hemispheres (*e–g*) at different eccentricities (Table 2). Spatial correlation values were contrast enhanced because they were of very low amplitude, ranging within ± 3 from mean gray (128) as indicated by the gray-scale bar. Scale bars: *a–c*, 1 mm; *d–g*, 100 μm.

Table 2. Distribution of MT-projecting neurons among CO columns in V1

Hemisphere	Eccentricity	Patch	Border	Interpatch	χ^2 *p* value*
Monkey 1, L	3°	126	140	113	0.24
Monkey 2, L	1°	106	120	127	0.38
Monkey 2, R	7°	186	170	180	0.69
Monkey 3, L	15°	232	227	204	0.36

*Three-way χ^2 test using a parcellation of V1 into patch, border, or interpatch zones of equal area.

Shipp and Zeki, 1989) and the only cells in layer 4B to receive a predominantly magnocellular input (via layer 4Cα) (Yabuta et al., 2001). Microelectrode recordings have shown that V1 cells projecting directly to MT are highly direction-selective (Movshon and Newsome, 1996). However, in this physiological study, their morphology was unknown.

The pyramidal cells of layer 4B receive both magnocellular and parvocellular inputs (Sawatari and Callaway, 1996; Yabuta et al., 2001) and form part of the population that projects to V2 (Rockland, 1992). With the present data, it appears that smaller layer 4B pyramidal cells are the main candidate for carrying parvocellular information into V2. Thus, not only is layer 4B one of the first layers in which orientation and direction selectivity are generated in V1, it may also be a key area for the segregation and distribution of these tuning features. The manifold cells, as a third group, are the only cells that send a common signal to extrastriate areas. Medium-sized pyramdial cells in the prefrontal cortex have been shown previously to send dual efferents (Schwartz and Goldman-Rakic, 1984), suggesting that this may be common cell morphology for manifold projections.

The projection from V1 to V2 thick stripes originates from interpatches (Sincich and Horton, 2002a), implying that a functional segregation exists between cells in patches and interpatches of layer 4B. In this context, note that layer 4B cells projecting to MT arise from interpatches and patches. A subpopulation of 4B cells, located in patches, therefore projects to MT but not the V2 thick stripes, which in turn project to MT. We can only speculate about the signal they carry. It has been suggested that patches mediate color processing in V1 (Livingstone and Hubel, 1984; Ts'o and Gilbert, 1988), although this idea is controversial (Edwards et al., 1995; Leventhal et al., 1995). If correct, the V1 patch cells in 4B projecting to MT may convey color information (Saito et al., 1989; Dobkins and Albright, 1994; Seidemann et al., 1999; Thiele et al., 2001).

Although we found no relationship between MT-projecting cells and CO patches, which is in agreement with a previous study (Shipp and Zeki, 1989), there does appear to be a correlation in some nocturnal primates. In the owl monkey and bushbaby, the direct V1 to MT projection is denser than in macaques and tends to originate in CO patches (Boyd and Casagrande, 1999). It is possible that a genuine species difference exists. However, the difference in density of the projection may be a confounding factor. We found a mean density of 50 cells per square millimeter in the macaque, whereas Boyd and Casagrande (1999) reported a mean density of 423 cells per square millimeter for the owl monkey and bushbaby combined. Boyd and Casagrande found a correlation with CO patches only for their cases with the densest labeling. This implies that a correlation might be difficult to detect in macaques because the 4B projection to MT is sparser. However, one case from Shipp and Zeki's macaque data was analyzed by Boyd and Casagrande (1999), who found a correlation at a density of 13 cells per square millimeter. Thus, some macaques may have more MT-projecting cells in CO patches, but in light of our additional data, we conclude that this clustering is not a general tendency among macaques.

Our findings modify the overall picture of interareal connec-

tions in the visual system. Connections have always been depicted as being formed unitarily by areas or layers; however, neurons are the basic projection units. We do not know how prevalent manifold projections are, in part because a functional relationship between injected sites (e.g., homotopy in sensory areas) is required to produce double labeling. Injections with dual tracers are seldom made into related portions of different cortical areas (Kennedy and Bullier, 1985; Morel and Bullier, 1990; Burton and Fabri, 1995). We injected the same retinotopic loci in V2 and MT and found that double-labeled cells averaged 6% of the MT-projecting neurons and 2.5% of the V2-projecting neurons, probably low estimates given the unknown efficiency of the tracers. Perhaps the most significant finding was that the populations of layer 4B solitary neurons projecting to either V2 or MT are different, on the basis of their distinct size histograms.

If the brain distributes signals using many segregated classes of solitary neurons and manifold neurons, conventional wiring schemes must be revised to incorporate an exponential increase in the number of potential information channels. Because every cortical area projects to many other areas, our results also emphasize that each "link" between the areas is composed of at least one solitary and one manifold connection. For example, a network of five areas fully connected with solitary axons would have $n(n-1) = 20$ links. This number jumps to $n^2(n-1)/2 = 50$ links, if one assumes that neurons in each area send a solitary axon or a manifold axon to two other areas. Because some neurons may target three or more areas, this equation does not account for the number of conceivable projections. Of course, not all of these projections need to exist. In a cortical scheme based on an $n(n-1)$ model, only 31% of the possible connections have been demonstrated (Felleman and Van Essen, 1991).

The small percentage of double-labeled cells that we found indicates that feedforward cortical projections, at least from V1, are predominately solitary. Solitary neurons also dominate feedback projections, but manifold neurons appear to be relatively more common (Salin and Bullier, 1995). For instance, the reconstruction of axons from tracer-filled MT cells showed that 2 of 20 terminated in both V1 and V2 (Rockland and Knutson, 2000). Another study found that 21–31% of the MT feedback neurons were double labeled after different retrograde tracers were injected at corresponding points in V1 and V2 (Kennedy and Bullier, 1985). Thus, it appears that V1 sends information to V2 and MT via primarily segregated channels but receives a substantial fraction of its feedback from MT via projections that are shared with V2.

The finding of three potential output channels from layer 4B of V1, in which, until recently, only a single channel was assumed (Livingstone and Hubel, 1988; Zeki and Shipp, 1988; Merigan and Maunsell, 1993; Van Essen and Gallant, 1994), provides a glimpse of the complexity of cortical connections. If each type of projection arising from a cortical area carries a unique signal (a reasonable assumption if form follows function), the signal handling capability of the brain is considerably enriched by the existence of multiple output streams from individual cortical layers.

References

Barbas H (1995) Pattern in the cortical distribution of prefrontally directed neurons with divergent axons in the rhesus monkey. Cereb Cortex 5:158–165.

Blasdel GG, Fitzpatrick D (1984) Physiological organization of layer 4 in macaque striate cortex. J Neurosci 4:880–895.

Boussaoud D, Ungerleider LG, Desimone R (1990) Pathways for motion analysis: cortical connections of the medial superior temporal and fundus of the superior temporal visual areas in the macaque. J Comp Neurol 296:462–495.

Boyd JD, Casagrande VA (1999) Relationships between cytochrome oxidase (CO) blobs in primate primary visual cortex (V1) and the distribution of neurons projecting to the middle temporal area (MT). J Comp Neurol 409:573–591.

Bullier J, Kennedy H (1987) Axonal bifurcation in the visual system. Trends Neurosci 10:205–210.

Bullier J, Kennedy H, Salinger W (1984) Branching and laminar origin of projections between visual cortical areas in the cat. J Comp Neurol 228:329–341.

Burton H, Fabri M (1995) Ipsilateral intracortical connections of physiologically defined cutaneous representations in areas 3b and 1 of macaque monkeys: projections in the vicinity of the central sulcus. J Comp Neurol 355:508–538.

Cragg BG (1969) The topography of the afferent projections in the circumstriate visual cortex of the monkey studied by the Nauta method. Vision Res 9:733–747.

DeYoe EA, Van Essen DC (1985) Segregation of efferent connections and receptive field properties in visual area V2 of the macaque. Nature 317:58–61.

Dobkins KR, Albright TD (1994) What happens if it changes color when it moves?: the nature of chromatic input to macaque visual area MT. J Neurosci 14:4854–4870.

Dow BM (1974) Functional classes of cells and their laminar distribution in monkey visual cortex. J Neurophysiol 37:927–946.

Edwards DP, Purpura KP, Kaplan E (1995) Contrast sensitivity and spatial frequency response of primate cortical neurons in and around the cytochrome oxidase blobs. Vision Res 35:1501–1523.

Felleman DJ, Van Essen DC (1991) Distributed hierarchical processing in the primate cerebral cortex. Cereb Cortex 1:1–47.

Gattass R, Gross CG (1981) Visual topography of striate projection zone (MT) in posterior superior temporal sulcus of the macaque. J Neurophysiol 46:621–638.

Gattass R, Gross CG, Sandell JH (1981) Visual topography of V2 in the macaque. J Comp Neurol 201:519–539.

Giolli RA, Towns LC (1980) A review of axon collateralization in the mammalian visual system. Brain Behav Evol 17:364–390.

Hawken MJ, Parker AJ, Lund JS (1988) Laminar organization and contrast selectivity of direction selective cells in the striate cortex of the Old-World monkey. J Neurosci 8:3541–3548.

Horton JC, Hubel DH (1981) Regular patchy distribution of cytochrome oxidase staining in primary visual cortex of macaque monkey. Nature 292:762–764.

Hubel DH, Wiesel TN (1968) Receptive fields and functional architecture of monkey striate cortex. J Physiol (Lond) 195:215–243.

Kennedy H, Bullier J (1985) A double-labeling investigation of the afferent connectivity to cortical areas V1 and V2 of the macaque monkey. J Neurosci 5:2815–2830.

Krubitzer LA, Kaas JH (1989) Cortical integration of parallel pathways in the visual system of primates. Brain Res 478:161–165.

Leventhal AG, Thompson KG, Liu D, Zhou Y, Ault SJ (1995) Concomitant sensitivity to orientation, direction, and color of cells in layers 2, 3, and 4 of monkey striate cortex. J Neurosci 15:1808–1818.

Livingstone MS, Hubel DH (1984) Anatomy and physiology of a color system in the primate visual cortex. J Neurosci 4:309–356.

Livingstone MS, Hubel DH (1988) Segregation of form, color, movement, and depth: anatomy, physiology, and perception. Science 240:740–749.

Llewellyn-Smith IJ, Minson JB, Wright AP, Hodgson AJ (1990) Cholera toxin B-gold, a retrograde tracer that can be used in light and electron microscopic immunocytochemical studies. J Comp Neurol 294:179–191.

Lockard I (1992) Desk reference for neuroscience, Ed 2. New York: Springer.

Lund JS, Lund RD, Hendrickson AE, Bunt AH, Fuchs AF (1975) The origin of efferent pathways from the primary visual cortex, area 17, of the macaque monkey as shown by retrograde transport of horseradish peroxidase. J Comp Neurol 164:287–303.

Maunsell JH, Van Essen DC (1983) The connections of the middle temporal visual area (MT) and their relationship to a cortical hierarchy in the macaque monkey. J Neurosci 3:2563–2586.

Merigan WH, Maunsell JHR (1993) How parallel are the primate visual pathways? Annu Rev Neurosci 16:369–402.

Meynert T (1872) Vom Gehirne de Säugethiere. In: Handbuch der Lehre von den Geweben des Menschen und der Thiere, Vol II (Stricker S, ed), pp 694–808. Leipzig, Germany: Engelmann.

Morel A, Bullier J (1990) Anatomical segregation of two cortical visual pathways in the macaque monkey. Vis Neurosci 4:555–578.
Movshon JA, Newsome WT (1996) Visual response properties of striate cortical neurons projecting to area MT in macaque monkeys. J Neurosci 16:7733–7741.
Nakamura H, Gattass R, Desimone R, Ungerleider LG (1993) The modular organization of projections from areas V1 and V2 to areas V4 and TEO in macaques. J Neurosci 13:3681–3691.
Olavarria JF, Van Sluyters RC (1985) Unfolding and flattening the cortex of gyrencephalic brains. J Neurosci Methods 15:191–202.
Rockland KS (1992) Laminar distribution of neurons projecting from area V1 to V2 in macaque and squirrel monkeys. Cereb Cortex 2:38–47.
Rockland KS, Drash GW (1996) Collateralized divergent feedback connections that target multiple cortical areas. J Comp Neurol 373:529–548.
Rockland KS, Knutson T (2000) Feedback connections from area MT of the squirrel monkey to areas V1 and V2. J Comp Neurol 425:345–368.
Saito H, Tanaka K, Isono H, Yasuda M, Mikami A (1989) Directionally selective responses of cells in the middle temporal area (MT) of the macaque monkey to the movement of equiluminous opponent color stimuli. Exp Brain Res 75:1–14.
Salin PA, Bullier J (1995) Corticocortical connections in the visual system: structure and function. Physiol Rev 75:107–154.
Sawatari A, Callaway EM (1996) Convergence of magno- and parvocellular pathways in layer 4B of macaque primary visual cortex. Nature 380:442–446.
Schiller PH, Finlay BL, Volman SF (1976) Quantitative studies of single-cell properties in monkey striate cortex. II. Orientation specificity and ocular dominance. J Neurophysiol 39:1320–1333.
Schwartz ML, Goldman-Rakic PS (1984) Callosal and intrahemispheric connectivity of the prefrontal association cortex in rhesus monkey: relation between intraparietal and principal sulcal cortex. J Comp Neurol 226:403–420.
Seidemann E, Poirson AB, Wandell BA, Newsome WT (1999) Color signals in area MT of the macaque monkey. Neuron 24:911–917.
Shipp S, Zeki S (1985) Segregation of pathways leading from area V2 to areas V4 and V5 of macaque monkey visual cortex. Nature 315:322–325.
Shipp S, Zeki S (1989) The organization of connections between areas V5 and V1 in macaque monkey visual cortex. Eur J Neurosci 1:309–332.
Sincich LC, Horton JC (2002a) Divided by cytochrome oxidase: a map of the projections from V1 to V2 in macaques. Science 295:1734–1737.
Sincich LC, Horton JC (2002b) Pale cytochrome oxidase stripes in V2 receive the richest projection from macaque striate cortex. J Comp Neurol 447:18–33.
Sincich LC, Horton JC (2002c) Double-labeling of the projections from striate cortex to extrastriate areas V2 and MT in the macaque monkey. Soc Neurosci Abstr 28:325.3.
Thiele A, Dobkins KR, Albright TD (2001) Neural correlates of chromatic motion perception. Neuron 32:351–358.
Tigges J, Tigges M, Anschel S, Cross NA, Letbetter WD, McBride RL (1981) Areal and laminar distribution of neurons interconnecting the central visual cortical areas 17, 18, 19, and MT in squirrel monkey (Saimiri). J Comp Neurol 202:539–560.
Tootell RBH, Taylor JB (1995) Anatomical evidence for MT and additional cortical visual areas in humans. Cereb Cortex 1:39–55.
Tootell RBH, Silverman MS, De Valois RL, Jacobs GH (1983) Functional organization of the second cortical visual area in primates. Science 220:737–739.
Ts'o DY, Gilbert CD (1988) The organization of chromatic and spatial interactions in the primate striate cortex. J Neurosci 8:1712–1727.
Ungerleider LG, Desimone R (1986) Cortical connections of visual area MT in the macaque. J Comp Neurol 248:190–222.
Ungerleider LG, Mishkin M (1979) The striate projection zone in the superior temporal sulcus of Macaca mulatta: location and topographic organization. J Comp Neurol 188:347–366.
Van Essen DC, Gallant JL (1994) Neural mechanisms of form and motion processing in the primate visual system. Neuron 13:1–10.
Van Essen DC, Maunsell JHR, Bixby JL (1981) The middle temporal visual area in the macaque: myeloarchitecture, connections, functional properties and topographic organization. J Comp Neurol 199:293–326.
Weller RE, Kaas JH (1983) Retinotopic patterns of connections of area 17 with visual areas V-II and MT in macaque monkeys. J Comp Neurol 220:253–279.
Wong-Riley MTT (1979) Changes in the visual system of monocularly sutured or enucleated cats demonstrable with cytochrome oxidase histochemistry. Brain Res 171:11–28.
Yabuta NH, Sawatari A, Callaway EM (2001) Two functional channels from primary visual cortex to dorsal visual cortical areas. Science 292:297–300.
Yukie M, Iwai E (1985) Laminar origin of direct projection from cortex area V1 to V4 in the rhesus monkey. Brain Res 346:383–386.
Zeki S, Shipp S (1988) The functional logic of cortical connections. Nature 335:311–317.
Zeki S (1969) Representation of central visual fields in prestriate cortex of monkey. Brain Res 14:271–291.